Observation of Field-Emission Dependence on Stored Energy

Jiahang Shao,[1,2,*] Sergey P. Antipov,[2,3] Sergey V. Baryshev,[2,3] Huaibi Chen,[1] Manoel Conde,[2] Darrell S. Doran,[2] Wei Gai,[2] Chunguang Jing,[2,3] Wanming Liu,[2] John Power,[2] Jiaqi Qiu,[2,3] Jiaru Shi,[1] Dan Wang,[1,2] Faya Wang,[4,†] Charles E. Whiteford,[2] Eric Wisniewski,[2] and Liling Xiao[4]

[1]*Department of Engineering Physics, Tsinghua University, Beijing 100084, People's Republic of China*
[2]*Argonne National Laboratory, Lemont, Illinois 60439, USA*
[3]*Euclid Techlabs LLC, Solon, Ohio 44139, USA*
[4]*SLAC National Accelerator Laboratory, Menlo Park, California 94025, USA*

(Received 24 August 2015; published 23 December 2015)

Field emission from a solid metal surface has been continuously studied for a century over macroscopic to atomic scales. It is general knowledge that, other than the surface properties, the emitted current is governed solely by the applied electric field. A pin cathode has been used to study the dependence of field emission on stored energy in an L-band rf gun. The stored energy was changed by adjusting the axial position (distance between the cathode base and the gun back surface) of the cathode while the applied electric field on the cathode tip is kept constant. A very strong correlation of the field-emission current with the stored energy has been observed. While eliminating all possible interfering sources, an enhancement of the current by a factor of 5 was obtained as the stored energy was increased by a factor of 3. It implies that under certain circumstances a localized field emission may be significantly altered by the global parameters in a system.

DOI: 10.1103/PhysRevLett.115.264802 PACS numbers: 29.20.Ej, 52.80.Pi, 79.70.+q

Field emission (also known as dark current) was discovered as a quantum phenomenon and is described by the well-known Fowler-Nordheim equation [1–5]. It plays an important role in high gradient dc and rf devices, cold cathode electron sources, and internal electron transfer processes in electronic devices [5]. In particular, field emission is considered to be the trigger of vacuum breakdowns in high gradient devices [3,6–9]. A better understanding of field emission will benefit the research and development for high gradient accelerating structures to be used in future linear colliders [10], x-ray free-electron lasers [11,12], compact medical and industrial linacs [13,14], etc. In earlier studies, field emission was considered to be dependent only on the applied electric field (with geometrical field enhancement factors or space charge effects) at the same surface conditions [1–5]. However, a recent theoretical study has suggested that field emission is essentially coupled to global parameters such as group velocity, frequency, and so on of a macroscopic system [15]. Moreover, an early experiment has revealed that the operational electric field depends strongly on the net power flow in a traveling wave X-band system [16]. In this Letter, we report how the dark current depends on the stored energy (or input power) in a standing wave cavity.

An L-band rf gun at Argonne Wakefield Accelerator facility (AWA) is used as a test bed for the study [17,18]. A pin cathode (Fig. 1) is installed to significantly enhance the electric field on the cathode to govern the field emission in the gun. The stored energy was changed by adjusting the recess of the cathode while the maximum electric field on the cathode tip (denoted as E_{tip}) is kept constant [19].

The cathode recess is adjusted by a micrometer. The position of the cathode inside the cavity is measured by the micrometer and confirmed by a direct measurement with a long stick inserted at the gun exit. The maximum error of the cathode position measurement is ~0.1 mm, which is acceptable for our study. The detuning of the gun by the cathode displacement was compensated by a tuner at the side of the gun. The maximum recess is ~6 mm, limited by the tuner range, which is ~6 MHz. When the cathode is pushed farther into the cavity, the electric field on the

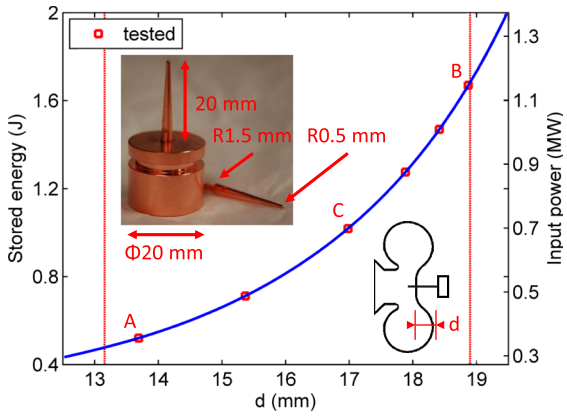

FIG. 1 (color online). Stored energy inside the cavity and input power for the same E_{tip} (625 MV/m) at different cathode positions. The red vertical lines show the cathode position boundaries in the experiment. Inset: Pin cathodes from SLAC.

 © 2015 American Physical Society

TABLE I. Parameters of the L-band photocathode gun.

Parameter	Value	
	Position A	Position B[a]
d (mm)[b]	13.7	18.9
Quality factor Q_0	12 850	13 730
ρ_{ext}[c]	1.36	1.47

[a]Positions A and B correspond to the minimum and maximum stored energy tested in the experiment, as illustrated in Fig. 1.
[b]Distance between the cathode base and the gun back surface.
[c]Coupling between the cavity and the waveguide.

cathode tip is enhanced so that a lower stored energy and input power are needed to maintain a constant E_{tip}, as illustrated in Fig. 1. The electromagnetic simulation of the cavity has been done in 2D with the Superfish code [20] and in 3D with the Omega3P code [21]. The results of the two simulations are consistent with each other. The cold test data are summarized in Table I.

The geometry of the cavity with a pin or a flat cathode is illustrated in Fig. 2(a). The electric field along the cavity surface simulated by Superfish is plotted in Fig. 2(b), where the surface field of the tip is much larger than any place else in the cavity. Accordingly, the majority of the field emission in the cavity is considered to originate from the tip. The corresponding magnetic field along the pin at both positions is less than 65 kA/m, leading to negligible pulse heating in the experiment [22].

Electrical contact between the cathode and the cavity is ensured by a spring located ~5.5 mm behind the cathode base. The low field at the ~0.03 mm gap leads to negligible field emission from this area.

The layout of the L-band photocathode test stand at AWA is shown in Fig. 3. Diagnostics involved in the experiment are a bidirectional coupler to monitor the input and reflected rf signals, an antenna (pickup) to monitor the rf signal inside the cavity, and a Faraday cup with an integrating circuit located at the exit of the gun to measure the dark current. A dark current imaging system is located downstream to index dark current emitters on the cathode with ~100 μm resolution. This consists of a solenoid, a collimator with small apertures, trim magnets, and yttrium-aluminum-garnet (YAG) screens [23]

Two identical pin cathodes, No. 07 and No. 15, have been tested in the experiment. Before the dark current measurement, both pins had been carefully conditioned up to $E_{tip} \sim 700$ MV/m at cathode position B (corresponding to the maximum stored energy). The parameters of the conditioning history are summarized in Table II.

After the conditioning, the repetition rate was dropped to 1 Hz and E_{tip} was kept below 660 MV/m to avoid any breakdown. Dark current was then measured at fairly consistent surface conditions. At each cathode position, the dark current was measured at different tip fields. The gun focusing solenoid was adjusted correspondingly to maximize the capture rate. For a given cathode position, the test usually took about 2 h and the dark current measurement was repeated under selected focusing solenoid strengths at the end to ensure that the surface conditions of the cathode had not changed. The No. 07 and No. 15 pin cathodes have been measured at six (positions A to B) and four (positions C to B) different positions, respectively, illustrated as red squares in Fig. 1, to confirm the observation.

There are two steps in the typical dark current signal as illustrated in the inset of Fig. 4. The first is caused by field emission. The second results from multipacting, which is

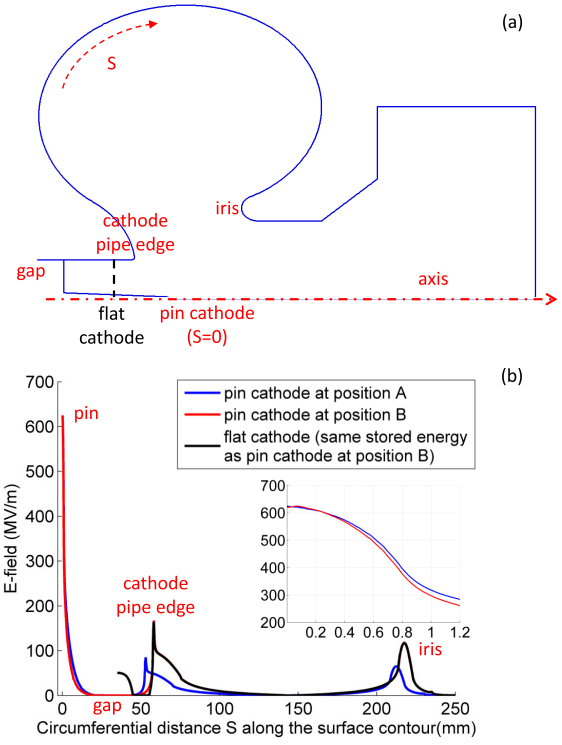

FIG. 2 (color online). (a) 2D geometry of the cavity (the pin cathode at position A or the flat cathode at its fixed position). (b) Electric field along the cavity surface contour (start from the pin). Inset: Zoom-in view at the tip.

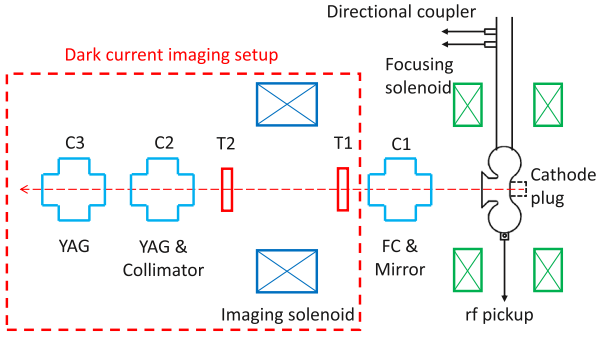

FIG. 3 (color online). Layout of the L-band photocathode test stand at AWA. FC, Faraday cup; C, cross; and T, trim.

TABLE II. Parameters of the pin cathodes' conditioning history. The difference in pulse length, flattop of electric field, and repetition rate is caused by different klystron and waveguide configurations.

Parameter	Value	
	No. 07	No. 15
Pulse length (μs)	8	6.5
Flattop of electric field (μs)	6.5	4.0
Repetition rate (Hz)	10	2
Total pulses	~190 000	~50 000
Number of breakdowns	~100	~30
Maximum E_{tip} (MV/m)	~700	

verified by two features reported by another group [24]: (1) the amplitude of this step is independent of the input power and (2) the delay t_{rear} between the start of this step and the end of the rf pulse follows the relation

$$E_{MP} = E_{max} \exp(-t_{rear}/\tau), \quad (1)$$

where τ is the fill or decay time of the cavity, E_{max} is the maximum field on the tip during the pulse, and E_{MP} is the field on the tip when the multipacting occurs. τ is obtained by fitting the data as 1.48 μs, which is in reasonable agreement with the value of ~1.33 μs deduced from the cold test results. In the following calculation and analysis, only the first step (field emission) is taken into account.

The standard Fowler-Nordheim plot for different cathode positions is shown in Fig. 4, where the corresponding different stored energies at E_{tip} of 625 MV/m are labeled. The nonlinear dependence at the low field end for the lowest two stored energies is considered to be caused by multipacting at the beginning or during the rf pulse. Based on a previous study by another group, this phenomenon is likely to occur when the surface field is very low where

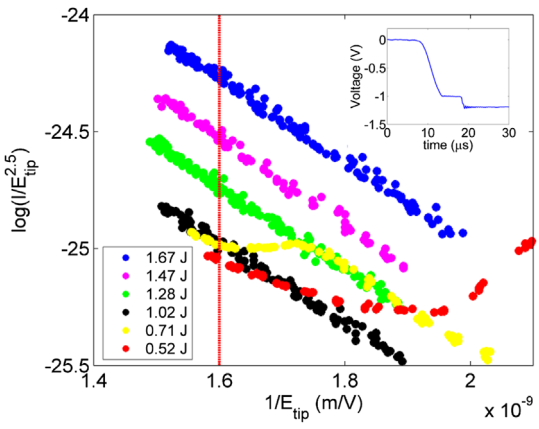

FIG. 4 (color online). Fowler-Nordheim plot of measured data from the No. 07 pin cathode. The red line indicates the interpolation point for the following data analysis. Inset: Typical Faraday cup signal after the integrating circuit.

resonant multipacting can be easily developed [24]. Because of the low time resolution of the integral Faraday cup signal, we cannot distinguish this particular multipacting current from the field-emission current. We examine the field-emission dependence on stored energy at E_{tip} of 625 MV/m, illustrated in Fig. 4 by the red dashed line, to minimize the influence from multipacting.

The collected dark current from the No. 07 and No. 15 pin cathodes at different positions (labeled by the different stored energies) and focusing solenoid strength at E_{tip} = 625 MV/m are shown in Figs. 5(a) and 5(b), respectively. Clearly, dark current at the same E_{tip} is enhanced when the stored energy is increased. In particular, a dark current enhancement by a factor of 5–20 is observed at various solenoid settings, while the stored energy is increased by a factor of 3.2 (1.67/0.52). Further on, the dark current capture ratio from the cathode tip to Faraday cup has been simulated with the ASTRA code [25]. We found that at a focusing solenoid strength of 625 G the capture ratio is consistent for the cathode at different positions [19]. The relative dark current (normalized to the current of the maximum stored energy) versus the stored energy is shown in Fig. 5(d) at this focusing strength. When the stored energy in the cavity is increased by threefold while keeping the same E_{tip}, the dark current will be enhanced by a factor of 5. The results from the two pin cathodes agree very well with each other.

Meanwhile, the field enhancement factor and emission areas of the four straight lines in Fig. 4 can be fitted based on the Fowler-Nordheim equation [3]. It is found that when the stored energy is increased by a factor of 1.6 (1.67/1.02, positions B to C as shown in Fig. 1), the field emission

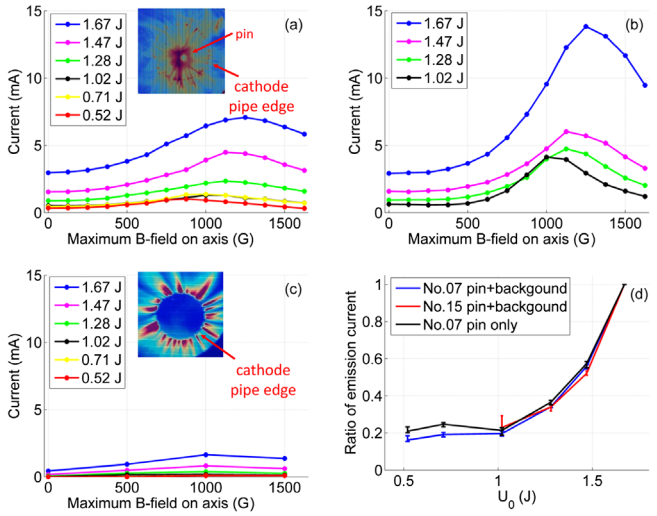

FIG. 5 (color online). (a)–(c) Captured dark current of the No. 07 and No. 15 pin cathodes at E_{tip} of 625 MV/m, and the flat cathode with different stored energies in the cavity. (d) Relative dark current with different stored energies. (a),(c) Insets: Dark current images with the pin and the flat cathode taken at the second cross (C2 as shown in Fig. 3).

factor remains ~15 while the emission area decreases from $\sim 8 \times 10^{-15}$ to $\sim 3 \times 10^{-15}$ mm^2. These observations are inconsistent with the Fowler-Nordheim theory, which predicts the same dark current at the same E_{tip} and the same surface conditioning. Possible mechanisms that may contribute to this observation have been examined.

(a) *Background emission from other surfaces.*—Although E_{tip} is kept constant for different stored energies by adjusting the cathode recess, the electric field on other parts of the cavity will be different and leads to different field-emission currents. To extract field emission from other places, a flat cathode was placed at ~2.9 mm behind the flush position to create the same surface fields on other cavity surfaces as in the case of the pin cathode, as shown in Fig. 2. The flat cathode was polished to a roughness of less than 20 nm with a diamond suspension. As the field on the flat cathode is 3.2 times lower than that on the cathode pipe edge, field emission will be dominated by the latter, which has been confirmed also by a previous dark current imaging experiment [23]. When the flat cathode is fixed at this position, the background emission was measured at different stored energies corresponding to those using the pin cathodes, as illustrated in Fig. 5(c). At the same focusing solenoid strength of 625 G (interpolated from the measured data), the dark current is about 5 times lower than that when the pin cathodes were present. From the insets in Fig. 5, the dominant field emission from the pin can also be vividly confirmed by the dark current images taken by the imaging system [23]. Thus background emission only leads to minor corrections to the observation, as illustrated in Fig. 5(d).

(b) *Secondary electron yield (SEY) from the Faraday cup.*—SEY from the Faraday cup strongly depends on the incident electron energy, and can lower the detected current [26]. To examine the effect on our observations, a dc bias voltage up to 500 V was applied to the Faraday cup to capture all the secondary electrons. When the stored energy is varied from 1.67 to 1.02 J (positions B to C as shown in Fig. 1), the maximum electron kinetic energy varies from ~1.6 to ~1.2 MeV. With the No. 15 pin cathode, SEY has been measured to increase from ~9% to ~13% correspondingly, which also leads to minor correction to the measurements.

(c) *Beam loading effect.*—Beam loading lowers the stored energy inside the cavity and has also been investigated [27]. The charge emitted during one rf cycle is less than 1 pC with maximum energy of ~0.9 MeV at the minimum stored energy (0.52 J), resulting in a beam power of 1.2 kW. As the input power is ~350 kW, the beam loading effect is negligible during the measurements.

(d) *Space charge limited emission.*—Space charge can lower the field emission remarkably and its effect can be characterized by the deviation from the Fowler-Nordheim equation at higher surface electric fields [28,29]. This has not been observed in this experiment (as illustrated in Fig. 4), so the space charge limited emission effect should not contribute to the phenomenon.

All the error mechanisms considered are insignificant to our main observations. The correlation of field emission current and stored energy may be fundamental. The observation is consistent with the recently developed model of macroscopic field emission, which describes how the microfield emission couples fundamentally with the global parameters of a system [15]. Based on the model, the surface field is the sum of the fields excited by the external rf source and those induced by the emission current, which strongly depends on the geometry of the cavity and is associated with global parameters (e.g., the stored energy in our case). Thus, when the position of the pin cathode changes, the self-induced field by the current will change accordingly. This will in turn lead to the variation of the field emission.

In summary, a strong correlation between the field-emission current and the stored energy has been observed on pin cathodes. This study has excluded mechanisms that may affect the conclusion, such as multipacting in the cavity, background emission from other surfaces, secondary electron emission from the Faraday cup, the beam loading effect, and the space charge limited emission effect. We conclude that the observation is fundamental and inconsistent with the Fowler-Nordheim equation. This indicates that macroscopic parameters like stored energy are affecting the microscopic emission. The findings suggest a new territory to be explored while developing field emission electron sources and high gradient devices.

We would like to thank the SLAC machine shop for preparing the pin cathodes, and Dr. Klaus Flöttmann from DESY for his great help with the ASTRA code and useful discussions. This work is supported by the U.S. Department of Energy Early Career Research Program under Contract Code LAB 11-572. The work by the AWA group is funded through the U.S. Department of Energy Office of Science under Contract No. DE-AC02-06CH11357, and the work at Tsinghua University is supported by National Natural Science Foundation of China under Grant No. 11135004.

*shaojh07@mails.tsinghua.edu.cn
†fywang@slac.stanford.edu

[1] R. H. Fowler and L. Nordheim, in *Proceedings of the Royal Society of London A: Mathematical, Physical and Engineering Sciences* (The Royal Society, London, 1928), Vol. 119, pp. 173–181.
[2] J. Gadzuk and E. Plummer, Rev. Mod. Phys. **45**, 487 (1973).
[3] J. W. Wang and G. A. Loew, SLAC Report No. 7684, 1997.
[4] G. N. Fursey, *Field Emission in Vacuum Microelectronics* (Springer Science and Business Media, Berlin, 2007).
[5] R. G. Forbes and J. H. Deane, Proc. R. Soc. A **463**, 2907 (2007).

[6] A. Grudiev, S. Calatroni, and W. Wuensch, Phys. Rev. ST Accel. Beams **12**, 102001 (2009).
[7] A. Descoeudres, Y. Levinsen, S. Calatroni, M. Taborelli, and W. Wuensch, Phys. Rev. ST Accel. Beams **12**, 092001 (2009).
[8] F. Wang, C. Adolphsen, and C. Nantista, Phys. Rev. ST Accel. Beams **14**, 010401 (2011).
[9] H. Chen *et al.*, Phys. Rev. Lett. **109**, 204802 (2012).
[10] CLIC Conceptual Design Report, type CERN Technical Report, 2012.
[11] "SwissFEL Conceptual Design Report," PSI Technical Report, 2010.
[12] Z. Zhao, S. Chen, L. Yu, C. Tang, L. Yin, D. Wang, and Q. Gu, in *Proceedings of IPAC2011 (the 2nd International Particle Accelerator Conference), San Sebastián, Spain* (JACoW, Geneva, 2011), THPC053.
[13] A. Degiovanni, in *Proceeding of 8th International Workshop on Breakdown Science and High Gradient Technology, Beijing, China* (2015).
[14] E. Tanabe, in *Proceeding of 6th International Workshop on Breakdown Science and High Gradient Technology, Tsukuba, Japan* (2012).
[15] F. Wang, in *Proceeding of 8th International Workshop on Breakdown Science and High Gradient Technology, Beijing, China* (Ref. [13]).
[16] F. Wang and Z. Li, in *Proceeding of the 4th International Particle Accelerator Conference, Shanghai, China* (JACoW, Geneva, 2013), WEPFI083.
[17] C. Ho *et al.*, in *Proceeding of the 6th European Particle Accelerator Conference, Stockholm, Sweden* (JACoW, Geneva, 1998), TUP33C.
[18] S. V. Baryshev, S. Antipov, J. Shao, C. Jing, K. J. P. Quintero, J. Qiu, W. Liu, W. Gai, A. D. Kanareykin, and A. V. Sumant, Appl. Phys. Lett. **105**, 203505 (2014).
[19] J. Shao *et al.*, in *Proceeding of the 6th International Particle Accelerator Conference, Richmond, VA* (JACoW, Geneva, 2015), WEPMN016.
[20] J. H. Billen and L. M. Young, Los Alamos National Laboratory Technical Report No. LA-UR-96-1834 (1996).
[21] K. Ko, A. Candel, L. Ge, A. Kabel, R. Lee, Z. Li, C. Ng, V. Rawat, G. Schussman, and L. Xiao, in *Proceeding of the 25th Linear Accelerator Conference, Tsukuba, Japan* (JACoW, Geneva, 2010), FR101.
[22] D. P. Pritzkau, RF Pulsed Heating, Ph.D. thesis, Stanford Linear Accelerator Center (2001).
[23] J. Shao *et al.*, in *Proceeding of the 6th International Particle Accelerator Conference, Richmond, VA, USA* (JACoW, Geneva, 2015), WEPMN015.
[24] J. H. Han, K. Flöttmann, and W. Hartung, Phys. Rev. ST Accel. Beams **11**, 013501 (2008).
[25] K. Flöttmann, ASTRA–A space charge tracking algorithm, DESY.
[26] J. S. Pearlman, Rev. Sci. Instrum. **48**, 1064 (1977).
[27] A. Chao, *Handbook of Accelerator Physics and Engineering* (World Scientific, Singapore, 1999).
[28] J. Barbour, W. Dolan, J. Trolan, E. Martin, and W. Dyke, Phys. Rev. **92**, 45 (1953).
[29] A. Rokhlenko, K. L. Jensen, and J. L. Lebowitz, J. Appl. Phys. **107**, 014904 (2010).